Position and Velocity Control of a Hybrid (Parallel-Seiral) Robot Manipulator for Propeller Grinding

Byung Oh Choi, Min Ki Lee*

KIMM, Changwon Univ*.

1. INTRODUCTION

The casting of a propeller blade cannot meet dimensional accuracy so that its surface must be ground. However, it is one of the least favored jobs because of dust, noise, vibration, and accidental injury. So, a serial robot manipulator has been applied to the grinding automation[1][2]. But its application is limited to light-load grinding works due to the poor stiffness of the manipulator. For high stiffness, Stewart first introduced a parallel manipulator, which also offers high accuracy and fast dynamic performance. Hence many researchers have studied different types of parallel manipulator for various applications[3][4]. Generally, they exhibit small workspace and complicated kinematics and dynamics. This paper introduces a Hybrid Robot Manipulator (HRM)[5] for propeller grinding, which yields large workspace and simplicity in kinematics. The HRM consists of a Serial Mechanism(SM) and a Parallel Mechanism(PM). The PM positioning a platform strengthens the stiffness, while the SM orienting the end effector enlarges the workspace.

The HRM is constructed and applied to propeller grinding. The inverse/direct kinematics and the Jacobian are implemented in real time position and velocity control. While the velocity control is used to measure an unknown geometric surface of a propelller blade, the position control is applied to grind the removal depth. This paper presents the performance of the HRM for propeller grinding and analyzed the force/moment acting at the passive and active joints.

2. HYBRID ROBOT MANIPULATOR

The HRM is made up of the PM and SM as shown in Fig. 1. The PM consists of three legs and a central axis. For i = 1,2,3, leg_i is connected from Bi to Pi through universal joints placed for $\| \overrightarrow{O_0 B_i} \| = r_B$ and $\| \overrightarrow{O_3 P_i} \| = r_P$. Bi and Pi are

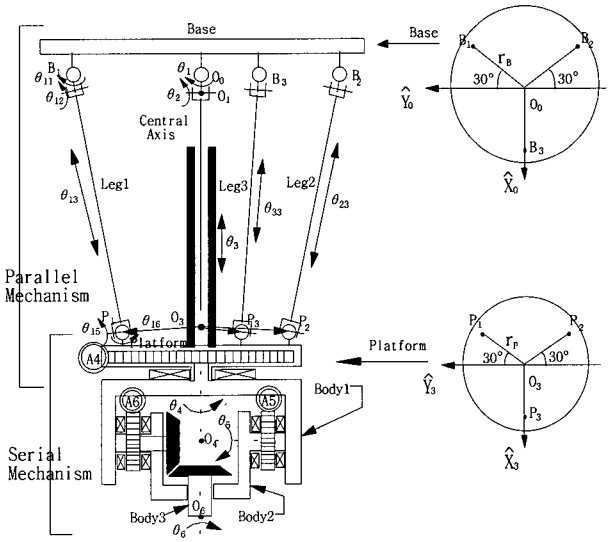

Fig. 1. Hybrid robot manipulator.

located symmetrically 120° apart and O_i(i = 0,3) are the central points of the base and platform. As shown in Fig. 2, the leg_i is a six degrees-of-freedom link train, which is composed of U_{i1} - n_{i1} - PR_{i2} - n_{i2} - U_{i3}. The upper universal joint, U_{i1}, provides two degrees of freedom (θ_{i1} and θ_{i2}), while the prismatic and rotary joint, PR_{i2}, yields another two degrees of freedom (θ_{i3} and θ_{i4}). Finally, two degrees of freedom (θ_{i5} and θ_{i6}) are added by the lower universal joint, U_{i3}. θ_{ij} (j = 1,2,4,5,6) are all passive joints but an active joint θ_{i3} shortens or extends the length of $\overrightarrow{B_i P_i}$ by a Linear Actuator (LA). To increase the ranges for θ_{i1} and θ_{i2}, an offset link is inserted in the upper universal joint, U_{i1}.

A central axis is located in the center to guide a platform along the axis constraining to the rotary motions (θ_1, θ_2) and the sliding motion (θ_3). The SM is mounted at the platform and designed for the wrist of the HRM producing the orientational motions (θ_4, θ_5, θ_6). That is, A_4 and A_5 rotate body_1 and body_2 by worm gears for motions θ_4

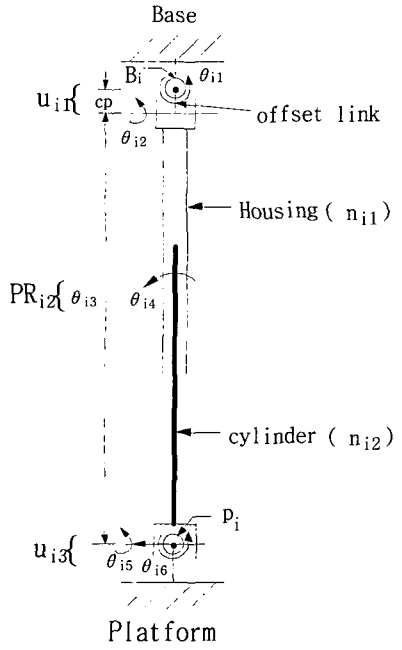

Fig. 2. Link train of leg_i.

and θ_5, respectively, and A_6 rotates body-3 (end-effector) through a bevel gear for θ_6. The ranges of θ_4 and θ_6 are 360° and that of θ_5 is within 270° so that the SM can compensate for the workspace which is limited by the PM. If the SM is included in the link train of the central axis, it is a six-degrees- of- freedom serial manipulator. That is, the upper joints θ_i(i = 1,2,3) position the SM and the rotary actuators θ_i(i = 4,5,6) orient the end effector.

3. INVERSE AND DIRECT KINEMATICS FOR POSITION CONTROL

To derive a kinematic model, we assign coordinates {i} to points O_i for i = 0,3,4 and 6 as shown in Fig. 1, For a given set of the joint displacements of a central axis, the position and orientation of the end effector is

$$(\overrightarrow{{}^0O_0O_6},\ {}^0R_6) = kin\_center(\theta_1, \cdots, \theta_6) \qquad (1)$$

where $\overrightarrow{{}^0O_0O_6}$ is the position vector from {0} to {6} and ${}^0R_6$ is a 3×3 rotation matrix of {6} with respect to {0}. The left superscript indicates the coordinate which describes the position vector or the rotation matrix. *kin_center* is the direct kinematics of the central axis, which is identical to that of a serial manipulator.

When the position and orientation of the end effector is given, *invkin_center* computes the joint displacements, i.e,

$$(\theta_1, \ldots, \theta_6) = Invkin\_center(\overrightarrow{{}^0O_0O_6},\ {}^0R_6) \qquad (2)$$

Here θ_i(i = 4,5,6) are directly rotated by the A_i but the passive joint θ_i(i = 1,2,3) are indirectly driven by the LA_i(i = 1,2,3). Now, we compute the length of LA_i. From the closed loops $O_0B_1P_1O_3$, $O_0B_2P_2O_3$ and $O_0B_3P_3O_3$ in the PM,

$$\overrightarrow{{}^0B_iP_i} = \overrightarrow{{}^0O_oO_3} - \overrightarrow{{}^0O_oB_i} + {}^0R_3\,\overrightarrow{{}^3O_3P_i}\ (i = 1,2,3) \qquad (3)$$

and the length of the LA_i is $\theta_{i3} = \| \overrightarrow{{}^0B_iP_i} \|$ unless the offset link is inserted. But they must be computed by the inverse kinematics of the link train of leg_i as shown below.

$$\theta_{i3} = Invkin\_leg\_i(\overrightarrow{{}^0B_iP_i}) \qquad (4)$$

Consequently, (2)-(4) are the inverse kinematics computing the active joint displacements.

Contrarily, the direct kinematics is to find the position and orientation for a given set of active joint displacements. θ_i (i = 4,5,6) are directly measured from rotary actuators but θ_i (i = 1,2,3) are determined by

$$\theta_i = const\_i(\theta_{13}, \theta_{23}, \theta_{33}) \qquad (5)$$

where $const\_i(\cdot)$ are the GC equations of the PM. In general, they are highly nonlinear equations with multiple solutions because link trains form multiple closed loops[6]. In the HRM, we can separate the position from the orientation without any extra sensor and induce the third order GC equation like (5) which is lower than that of the Stewart Platform. If the joints of the central axis are measured with extra sensors, the direct kinematics will be directly found by (1).

In order to derive the GC equations, we investigate the GC motions in the PM. From (1), $kin\_center(\theta_1, \theta_2, \theta_3)$ yields

$$\overrightarrow{{}^0O_0O_3} = \{\theta_3 s\theta_2, -s\theta_1(cp + \theta_3 c\theta_2), c\theta_1(cp + \theta_3 c\theta_2)\} \qquad (6)$$

and from $kin\_leg\_i\ (\theta_{i1}, \theta_{i2}, \theta_{i3})$ which is the direct kinematics of leg_i, we get

$$\overrightarrow{{}^0B_iP_i} = \{\theta_{i3} s\theta_{i2},\ -s\theta_{i1}(cp + \theta_{i3} c\theta_{i2}),\ c\theta_{i1}(cp + \theta_{i3} c\theta_{i2})\} \qquad (7)$$

Since $\overrightarrow{{}^0O_0O_3}$ is located in the center of the platform, and Bi and Pi are symmetrically 120° apart, the relation of $\overrightarrow{B_iP_i}$ and $\overrightarrow{{}^0O_0O_3}$ is

$$\overrightarrow{{}^0O_0O_3} = 1/3 \sum_{i=1}^{3} \overrightarrow{{}^0B_iP_i} \qquad (8)$$

which represents three GC equations including nine

unknowns such as θ_i, θ_{i1} and θ_{i2} for i = 1,2,3. Thus we need six more GC equations as follows: From the closed loops $O_0O_3P_1B_1$ and $O_0O_3P_2B_2$, $\overrightarrow{{}^0P_1P_2}$ is determined by

$$\begin{aligned}\overrightarrow{{}^0P_1P_2} &= (\overrightarrow{{}^0O_0B_2} + \overrightarrow{{}^0B_2P_2}) - (\overrightarrow{{}^0O_0B_1} + \overrightarrow{{}^0B_1P_1}) \\ &= {}^0R_3(\overrightarrow{{}^3O_3P_2} - \overrightarrow{{}^3O_3P_1})\end{aligned} \tag{9}$$

Correspondingly, from the closed loops, $O_0O_3P_2B_2$ and $O_0O_3P_3B_3$, $\overrightarrow{{}^0P_2P_3}$ is

$$\begin{aligned}\overrightarrow{{}^0P_2P_3} &= (\overrightarrow{{}^0O_0B_3} + \overrightarrow{{}^0B_3P_3}) - (\overrightarrow{{}^0O_0B_2} + \overrightarrow{{}^0B_2P_2}) \\ &= {}^0R_3(\overrightarrow{{}^3O_3P_3} - \overrightarrow{{}^3O_3P_2})\end{aligned} \tag{10}$$

To simplify the equations, the following variables are defined as

$$\begin{aligned} cb_i &= \theta_{i3}\, c\theta_{i2}, & sb_i &= \theta_{i3}\, s\theta_{i2} \\ ss_i &= (cp + cb_i)\, s\theta_{i1}, & cc_i &= (cp + cb_i)\, c\theta_{i1} \end{aligned}$$

where $c(\cdot) = \cos(\cdot)$ and $s(\cdot) = \sin(\cdot)$. Substituting the variables into GC (8)-(10), we solve for them. Then the definitions of ss_i and cc_i yield

$$cb_i = \pm\sqrt{ss_i^2 + cc_i^2} - cp \tag{11}$$

$$\begin{aligned}
&-p_1 c\theta_1 - p_2 c\theta_2 + p_3\theta_3 c\theta_2 + p_4 s\theta_1 + p_5 s\theta_2 + p_6\theta_3 s\theta_2 + p_7 s\theta_1 s\theta_2 + p_8\theta_3 c\theta_2 s\theta_1 + \theta_3^2 - \\
&cp\sqrt{(-q_1 c\theta_1 + q_2\theta_3 c\theta_2 + 4\theta_3^2 c\theta_2^2 + q_4 s\theta_1 + q_5 s\theta_2 + q_6 s\theta_1 s\theta_2 + q_7 s\theta_2^2 + q_8\theta_3 c\theta_2 s\theta_2 + q_9\theta_3 c\theta_2 s\theta_1 + c_s)} + c - \theta_{13}^2 = 0 \\
&-p_1 c\theta_1 - p_2 c\theta_2 + p_3\theta_3 c\theta_2 - p_4 s\theta_1 + p_5 s\theta_2 + p_6\theta_3 s\theta_2 - p_7 s\theta_1 s\theta_2 - p_8 c\theta_2\theta_3 s\theta_1 + \theta_3^2 - \\
&cp\sqrt{(-q_1 c\theta_1 + q_2\theta_3 c\theta_2 + 4\theta_3^2 c\theta_2^2 - q_4 s\theta_1 - q_5 s\theta_2 - q_6 s\theta_2 s\theta_2 + q_7 s\theta_2^2 + q_8\theta_3 c\theta_2 s\theta_1 + q_9\theta_3 c\theta_2 s\theta_2 + c_s)} + c - \theta_{23}^2 = 0 \\
&-4p_2 c\theta_2 + p_3 c\theta_2\theta_3 - p_4 s\theta_1 - 2p_6\theta_3 s\theta_2 + p_{35} s\theta_2\theta_3^2 - \\
&cp\sqrt{(-q_1 c\theta_1 + q_2\theta_3 c\theta_2 + 4\theta_3^2 c\theta_2^2 - q_4 s\theta_1 + q_5 s\theta_2 - q_6 s\theta_1 s\theta_2 + q_7 s\theta_2^2 + q_8 c\theta_2\theta_3 s\theta_2 - q_9 c\theta_2\theta_3 s\theta_1 + c_s)} + c - \theta_{33}^2 = 0
\end{aligned} \tag{12}$$

where

$$p_1 = \frac{3}{2} r_B r_P,\quad p_2 = \frac{1}{2} r_B r_P,\quad p_3 = 2cp,\quad p_4 = \sqrt{3} cp r_B,\quad p_5 = cp r_P,\quad p_6 = r_B,\quad p_7 = \frac{1}{2}\sqrt{3} r_B r_P,\quad p_8 = \sqrt{3} r_B$$

$$q_1 = 6 r_B r_P,\quad q_2 = 8cp,\quad q_4 = 4\sqrt{3} cp r_B,\quad q_5 = cp r_P,\quad q_6 = 2\sqrt{3} r_B r_P,\quad q_7 = r_P^2,\quad q_8 = 4 r_P,\quad q_9 = 4\sqrt{3} r_B$$

$$c = r_P^2 + r_B^2 + 2cp^2,\quad c_s = 4cp^2 + 3r_B^2 + 3r_P^2$$

cb_i are always positive since $-90° < \theta_{i2} < 90°$. So, we can take only a positive square root for a unique solution and derive three GC equations from $cb_i^2 + sb_i^2 - \theta_{i3}^2 = 0$ as shown below.

These are the third order simultaneous equations to compute θ_i(i = 1,2,3) for a set of θ_{i3}(i = 1,2,3). However, the GC equations are not expressed in explicit forms so that Newton's numerical method is employed to finding the solutions. For the high rate of convergence, approximate closed form solutions are obtained from the simplified PM and used for the initial values of the iterative computations.

Simplifying the PM with cp=0 and $r_p = 0$ induces the GC equations. Now, we can find the closed form solutions θ_i denoted by θ_i^0 and rewrite the (12) as

$$F[X] = 0 \tag{13}$$

where $X = [\theta_1, \theta_2, \theta_3]^T$. The classical Newton's method for the solution yields

$$X^{k+1} = X^k - \left[\frac{\partial F(X^k)}{\partial X}\right]^{-1} F(X^k) \tag{14}$$

Once finding real roots $X = [\theta_1, \theta_2, \theta_3]^T$, we substitute θ_i(i = 1,2,3) and θ_i(i = 4,5,6) into (1) to compute the position and orientation of the end effector.

4. JACOBIAN MATRIX FOR VELOCITY CONTROL

For a tool based control, a Jacobian matrix must be derived to transform the velocity of the tool to the actuators. Screw's theory(7) is applied to the Stewart Platform to obtain a 6×6 square Jacobian matrix which transforms six components (linear and rotary) of velocity of the platform to six actuators. But the PM of the HRM is supported by three actuators and a central axis. Hence, six components of velocities can not be directly transformed to three actuators. Here we use the motor algebra(8) to get the formulations for velocity transformation in the PM and SM, and combine them to find an entire Jacobian. When the j-joint θ_{ij} of i-link train is actuated by a unit velocity, the linear and rotary velocities of the point "o" in a platform are V and Ω, respectively. Then the motor vector of j-joint of i-link train is defined as

$${}^0M_{ij} = [V_x\ V_y\ V_z\ \Omega_x\ \Omega_y\ \Omega_z]^T \tag{15}$$

where the left superscript indicates the point where the velocities are inspected and the right subscripts i and j represent the link train and the joint,

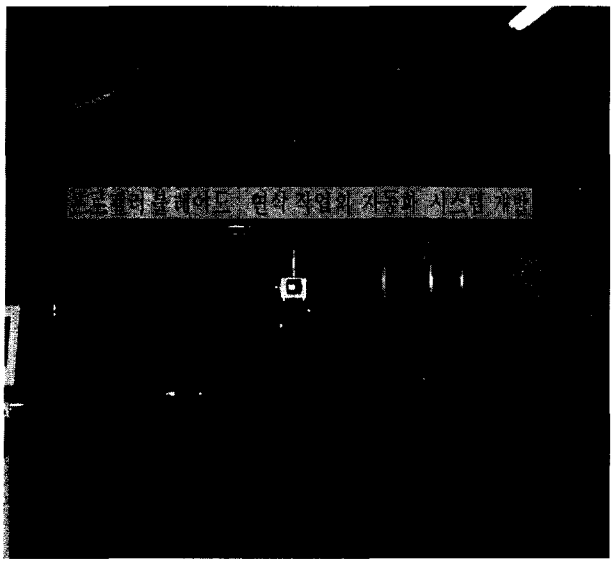

Fig. 3. The HRM constructed for propeller grinding.

respectively. From the definition, the velocity of the end effector is

$$vel\_O_6 = \dot{\theta}_1\, {}^{O_6}M_{c1} + \dot{\theta}_2\, {}^{O_6}M_{c2} + \cdots + \dot{\theta}_6\, {}^{O_6}M_{c6} \quad (16)$$

where vel_O_6, which is a 6×1 vector, represents a linear and rotary velocity of the point O_6 assigned to the end effector. For j = 1,2,$\cdots$,6, ${}^{O_6}M_{cj}$ is the motor of joint-j of central axis and $\dot{\theta}_i$ is the joint velocity. For a given vel_O_6 and ${}^{O_6}J_c = [\, {}^{O_6}M_{c1}\ {}^{O_6}M_{c2}\ \cdots\ {}^{O_6}M_{c6}]$, the joint velocities of the central axis are obtained by

$$\dot{\Theta} = {}^{O_6}J_c^{-1}\ Vel\_O_6 \quad (17)$$

where $\dot{\Theta}=[\,\dot{\Theta}_c\ \dot{\Theta}_s]^T$ in which $\dot{\Theta}_c=[\,\dot{\theta}_1, \dot{\theta}_2, \dot{\theta}_3]^T$ and $\dot{\Theta}_s=[\,\dot{\theta}_4, \dot{\theta}_5, \dot{\theta}_6]^T$. $\dot{\Theta}_s$ can be actively generated but $\dot{\Theta}_c$ must be driven by $\dot{\theta}_{i3}$ of LA_i. To find $\dot{\theta}_{i3}$ for i = 1,2,3, the output linear velocity of the link train of leg_i is computed by

$$[vel\_P_i]_V = \dot{\theta}_1 [\, {}^{p_i}M_{c1}]_V + \dot{\theta}_2 [\, {}^{p_i}M_{c2}]_V + \dot{\theta}_3 [\, {}^{p_i}M_{c3}]_V \quad (18)$$

Correspondingly, $[vel\_P_i]_V$ can be written as

$$[vel\_P_i]_V = \dot{\theta}_{i1} [\, {}^{p_i}M_{i1}]_V + \dot{\theta}_{i2} [\, {}^{p_i}M_{i2}]_V + \dot{\theta}_{i3} [\, {}^{p_i}M_{i3}]_V \quad (19)$$

Since the point P_i is located in the direction of LA_i, $[vel\_P_i]_V$ is projected to $\dot{\theta}_{i3}$ by $[\, {}^{p_i}M_{i3}]_V$, i.e.,

$$\dot{\theta}_{i3} = [\, {}^{p_i}M_{i3}]_V^T\, [vel\_P_i]_V \quad (20)$$

With $[\, {}^{p_i}J_c]_V = [[\, {}^{p_i}M_{c1}]_V [\, {}^{p_i}M_{c2}]_V [\, {}^{p_i}M_{c3}]_V]$, combining (17), (18) and (20) yields

$$[\, \dot{\theta}_{13}\ \dot{\theta}_{23}\ \dot{\theta}_{33}\ \dot{\theta}_4\ \dot{\theta}_5\ \dot{\theta}_6]^T = A\ B\ {}^{O_6}J_c^{-1}\ vel\_O_6 \quad (21)$$

where A and B are 6×12 and 12×6 matrices, respectively, as shown below:

$$A = \begin{bmatrix} [\, {}^{p_1}M_{13}]_V^T & 0\ 0\ 0 & 0\ 0\ 0 & \\ 0\ 0\ 0 & [\, {}^{p_2}M_{23}]_V^T & 0\ 0\ 0 & 0_{3\times3} \\ 0\ 0\ 0 & 0\ 0\ 0 & [\, {}^{p_3}M_{33}]_V^T & \\ \multicolumn{3}{c}{0_{3\times9}} & I_{3\times3} \end{bmatrix},$$

$$B = \begin{bmatrix} [\, {}^{p_1}J_c]_V & 0_{3\times3} \\ [\, {}^{p_2}J_c]_V & 0_{3\times3} \\ [\, {}^{p_3}J_c]_V & 0_{3\times3} \\ 0_{3\times3} & I_{3\times3} \end{bmatrix}$$

Therefore, an entire square Jacobian matrix is

$$J = A\ B\ {}^{O_6}J_c^{-1} \quad (22)$$

which can directly transform the velocity of the tool to actuators. If the offset links are short to be neglected, $[\, {}^{p_i}M_{i3}]_V$ is the unit vector in the direction of $\overrightarrow{B_iP_i}$, i.e.,

$$[\, {}^{p_i}M_{i3}]_V = \frac{\overrightarrow{B_iP_i}}{\| \overrightarrow{B_iP_i} \|} \quad (23)$$

This can remarkably reduce the computations but produce the velocity errors if the offset links are long.

5. POSITION AND VELOCITY CONTROL FOR PROPELLER GRINDING

As shown in Fig. 3, the HRM is constructed for propeller grinding. Before grinding the propeller blade, we decide removal depths by measuring the height of a casting blade. A touch probe is attached to an end effector and the X-Y plane of the blade is sliced into grids. A robot moves the touch probe in Z- direction at the points of the grids until it touches the surface. At a moment when the probe touches the surface, the controller decelerates to stop a robot and record current position data for measuring the height. For these measurements, we use a velocity control to move a robot in x-, y-, and z- directions when the corresponding keys are

pressed. In the velocity control, the duration for decelerating is short and consistent so that we can get correct data. However, it must include many computations for Jacobian, velocity mapping and the direct kinematics. The efficient algorithms derived in the previous sections are implemented in a real time control.

The controller moves the robot until the probe touches the surface. When the probe touches the surface, the controller stops the robot and saves the position data {x,y,z}. After these measurements are conducted at all the points of the grid, the casting surface is modeled by connecting the measured data. The normal direction of the modeled surface becomes an orientational data (Yaw, Pitch, Roll) in which a robot approaches for grinding. By comparing the measured dimension with the desired one, we determine the removal depth. Then a position control is used to grind the casting blade surface by interpolating the measured data with smooth curves. If the position and orientation of an end effector is declared as

$$p\_i = \{\{X, Y, Z\}, \{Yaw, Pitch, Roll\}\}$$

The position control process is sequentially performed. The robot moves along the path which is made up of the data stored between the start_point_list and the end_point_list. For point to point motion, only two data (p_start and p_end) are stored but for the continuous motion, intermediate data are interpolated by

$$p\_i = p\_start + (p\_end - p\_start)^{*} i/N \quad (i = 0,1,..,N) \qquad (24)$$

N is the interpolating number, which is decided from the grinding grade. The larger number N is, the higher grade the grinding work is. According to the p_i, active joint displacements are computed by the inverse kinematics, and they are converted into motor pulses for position commands to servo motors. The position control is relatively simple but cannot stop the robot until all the stored data are executed. Hence it shouldn't be used for measuring data, which requires to stop the robot at the moment when the probe touches the surface.

6. RESULTS

The velocity control is executed to measure the height of the point where a blade surface will be ground. Deviations from the desired path are within 0.7mm convincing an allowable accuracy(1 - 2mm) for the propeller grinding. The probe stops at the moment when it touches the blade surface. Table I presents the computational time of a PC Pentium-75 including the offset links. A total time of 4.88m-sec is fast enough to be implemented in a real time control but the burden of the computation is caused by a Jacobian. However, we can reduce it to 3.0m-sec by neglecting an offset link since its length is 20 mm, which is very short comparing with the length of LA_i (1038 - 1788mm). Due to the rapid computation, the errors are decreased even though the velocity error exists by ignoring the offset link. After measuring the height of the casting surface every 100mm which is distance between grids, we modeled the surface as shown in Fig. 4.

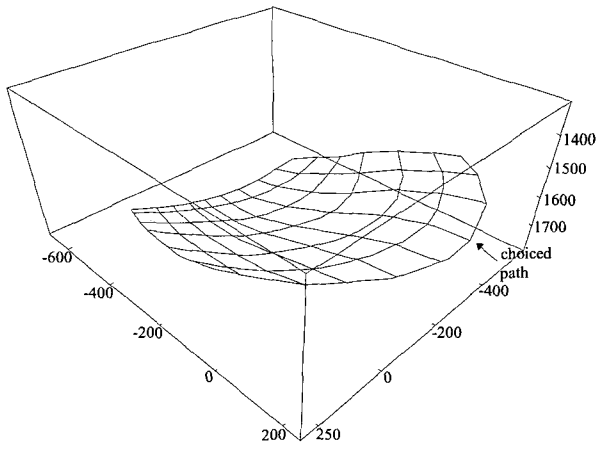

Fig. 4. Propeller blade surface modeling by measured data.

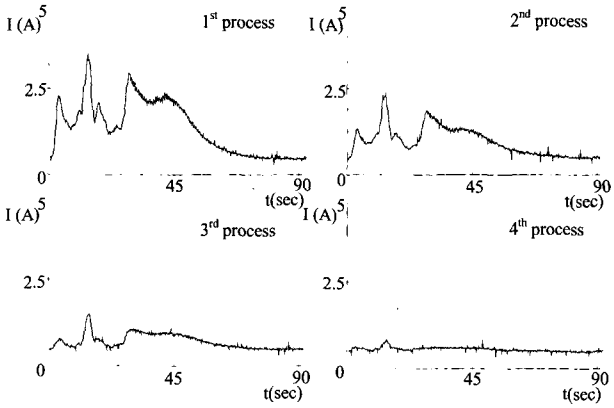

Fig. 5. Grinding load for each process.

A position control is conducted for the grinding work several times with the optimal selection of a grinder, a speed, a load and a removal depth. Fig. 5 presents the currents provided at the grinder when the surface was ground with 1mm-removal depth. The currents are extremely varied at the first process but they become stable. This is caused by the error in the model of the casting surface. For the stable grinding, the surface must be modeled as

Table 1. Computational time

Step	Process	Computation Time(msec)
1	Initial Value X^0, J^0	0.05
2	Newton's Iteration $\|F(X^{k+1})\| < error$	1.25
3	Direct Kinematics of Central Axis $kin\_center(\theta_1, \theta_2, .., \theta_6)$	0.21
4	Jacobian $J = ABJ_c^{-1}$	2.27
5	Active joint velocities $J \cdot Endvel$	1.10
	Total	4.88

accurate as possible and the small removal depth be selected. Once the process is done, the accomplishment is evaluated and the next process is followed. When the grinding work is completed, the errors by the position control are within 0.1mm, which makes it possible to do fine grinding works.

7. CONCLUSION

This paper introduced a hybrid parallel-serial robot manipulator with high stiffness and large workspace for propeller grinding. For the development of the robot system, inverse/ direct kinematics and Jacobian are derived and implemented in a real time control. By decoupling the motion of the PM from that of the SM, the geometric constraint is expressed by the third order simultaneous equation which has a unique solution. The motor algebra is applied to derive the formulations for the velocity transformation in the link train of leg_i and the central axis and they are combined to the entire Jacobian matrix.

The velocity control is successfully performed to measure the dimension of the propeller blade and the position control is conducted to grind the removal depth. The results show that the errors in the measuring and grinding process are within 0.5 mm meeting an allowable accuracy of propeller grinding. It is concluded that the hybrid parallel-serial manipulator is suitable for the propeller grinding and other machining works.

REFERENCES

[1] Whitney, D. E., and Tung, E. D., "Robot Grinding and Finishing of Cast Iron Stamping Dies," *ASME J. of Dynamic System, Measurement, and Control*, vol. 114, no. 1, pp. 132-140. 1992.

[2] Her, M. G. and Kazerooni, "Automated Robotic Deburring of Parts Using Compliance Control," *ASME J. of Dynamic System, Measurement, and Control*, vol. 113, pp. 60-66. 1991.

[3] D. R. Kerr, "Analysis, properties, and design of a Stewart platform transducer," *ASME J. of Mechanisms, Transmissions, and Automation in Design*, vol. 111, pp. 25-28, 1989.

[4] F. Pierrot, A. Foumier, and P. Dauchez, "Toward a fully parallel 6-DOF robot for high-speed applications," *IEEE J of Robotics and Automation*, vol. 7, pp. 15-22, 1992.

[5] 이민기, 최병오, 정종윤, 박근우, "프로펠러 연삭 작업을 위한 병렬-직렬 로봇암의 개발", 대한정밀공학회지, 제13권, 제2호, pp. 146-158, 1996.

[6] J. P. Merlet, "Direct Kinematics of Parallel Manipulators," *IEEE Trans. on Robotics and Automation*, vol. 9, no. 6, pp. 842-846, 1993

[7] M. G. Mohamed and J. Duffy, "A Direct Determination of the Instantaneous Kinematics of Fully Parallel Robot Manipulators," *ASME J. of Mechanisms, Transmissions, and Automation in Design*, vol.107, pp. 226-229, 1985.

[8] K. Sugimoto, "Kinematic and Dynamic Analysis of Parallel Manipulators by Means of Motor Algebra", *ASME J. of Mech., Trans., and Auto. in Design*. vol. 109, pp. 3-7, 1987.

저자소개

이 민 기(李敏基)

1955년 6월17일생

1982년 인하 대학교 기계공학과 졸업(학사)

1985년 미국 West Virginia Univ. 기계공학과 졸업(석사)

1988년 미국 West Virginia Univ. 기계공학과 졸업(박사)

1982년 - 1983년 한양주택(주) 사원

1988년 - 1990년 LG 산전 (주) 선임 연구원

1990년 - 현재 창원대학교 제어계측공과 부교수

<연구분야>

- 병렬기구 로봇 설계 및 제어
- 고 강성 로봇을 이용한 기계가공 자동화
- 병렬기구를 적용한 지능형 공작기계